Special Feature: Metal Forming and Processing

Research Report

Solidification Analysis of Al-Si Eutectic Alloy with Consideration of Undercooling and Solidification Rate

Jun Yaokawa, Yasushi Iwata, Norihiro Amano and Takashi Nakamichi

Report received on Feb. 25, 2015

ABSTRACT This paper describes a new solidification analysis technique based on the modified temperature recovery method that can calculate the undercooling during the solidification of Al-Si eutectic alloys. The solidification rate from an undercooled melt was considered using an empirical relationship between the undercooling and the solidification rate combined with a solidification rate parameter N that expresses the limitations of nucleation and growth at the early and last stages of solidification. The validation of the proposed technique was confirmed by comparing the experimental results for the time-dependent temperature distribution and the solid fraction distribution with the calculated results.

KEYWORDS Al-Si Alloy, Solidification Analysis, Eutectic, Solidification, Undercooling, Solidification Rate, Temperature Recovery Method

1. Introduction

By the 1980s, the use of aluminum alloy castings had increased drastically for the weight reduction of automobiles. Presently, many aluminum alloy components with complicated shapes are made by die-casting or other casting processes. Al-Si alloys are mainly used for these castings due to their good castability. However, improper casting conditions will cause casting defects and decrease the die life. To easily determine the appropriate casting conditions, one must understand the formation mechanism of the casting defects and develop more useful numerical simulation techniques.

Porosities and shrinkage cavities appearing on the machined surfaces of castings are the most crucial casting defects. Recently, it was reported that there are two types of eutectic solidification modes in Al-Si alloys that affect the formation of porosities and shrinkage cavities, i.e., the skin formation mode and the eutectic cell formation mode.[1,2] The latter mode is observed when the condition is satisfied that has a small temperature gradient, an undercooling of the melt, and the existence of sufficient nucleation sites. Undercooling also plays an important role in the growth of the eutectic cells. Nevertheless, almost none of the commercial casting simulation software take into account the undercooling in dealing with solidification phenomena. Therefore, it is desired to develop some simulation techniques that can consider the undercooling of the melt when treating the solidification of Al-Si alloys without much increase in the calculation time.

It has been reported that the undercooling of the melt during eutectic solidification increases with an increase in the cooling rate[3] and the purity of the melt.[4,5] The modification treatment of the melt by sodium or strontium additions also increases the undercooling.[6] For a small temperature gradient in the melt, the skin formation mode is found by the addition of sodium, whereas the cell formation mode is observed by the addition of strontium.[1,7,8] The change in these solidification modes depends on the conditions of the nucleation and growth of eutectic alloys.[7]

In the numerical simulation of solidification, the cell automaton method used for predicting solidification structures is a popular calculation technique that considers the undercooling of the melt. However, this method usually does not meet the requirements for the memory size and calculation time in practical uses. On the other hand, Koroyasu reported on a modified temperature recovery method that can consider the solidification of an undercooled melt.[11] Because of its simple calculation scheme, the calculation rate of this method seems to be as fast as that of the conventional calculation methods, and the modified temperature recovery method is available for many alloy systems. However, this method needs to be re-modified

in calculating the solidification rate because the nucleation and growth of the solid phase are not taken into account.

This research was carried out to develop a solidification analysis technique for Al-Si eutectic alloys that can consider the undercooling of the melt and the solidification rate without an increase in calculation time. For this purpose, the solidification behavior of a commercial grade Al-Si binary eutectic alloy was investigated at first. The temperature distribution, the solid fraction distribution, and the undercooling during the eutectic solidification of the alloy were determined by measuring the cooling curves and the solidification structure at various cooling rates. From these data, the solidification rate of the alloy was successfully derived. After that, a new calculation technique based on the modified temperature recovery method was proposed to consider the nucleation and growth from the undercooled melt. Its validation was confirmed by comparing the experimental and calculated temperature distributions and solid fraction distributions.

2. Experimental Procedure and Solidification Analysis

2. 1 Experiment

The Al-Si binary eutectic alloy was prepared from 99.9 mass% commercial grade aluminum and a commercial grade Al-25%Si alloy. The chemical composition of the alloy used in this study is listed in **Table 1**. About 1.5 kg of the eutectic alloy was melted and heated up to 1023 K in a clay bonded carbon crucible by an electric resistance furnace. A flux treatment and a hexachloroethane (C_2Cl_6) treatment were conducted to remove inclusions and dissolved hydrogen. After a 10 minute hold, the oxide film on the melt surface was swept out. Then, the melt was cooled to 973 K and poured into a shell-sand cup 30 mm in diameter and 50 mm in height for the cooling curve measurement at slow cooling rates (hereafter called the first measurement). In the first measurement, the cooling curves were obtained using a chromel-alumel thermocouple 0.3 mm in diameter placed at the center of the shell-sand cup. The initial temperature of the shell-cups was varied from room temperature to 573 K to obtain cooling curves for solidification times from 200 to 1000 s.

Table 1 Chemical composition of Al-Si alloy used in this study. (mass%)

Si	Cu	Mg	Zn	Fe	Cr	Mn	Ni	Pb	Sn	Al
12.8	0.01	0.01	0.01	0.12	<0.01	0.01	<0.01	<0.01	<0.01	bal.

Cooling curves at high cooling rates were obtained by the second measurement shown in **Fig. 1**. In the second measurement, cylindrical ingots 10 mm in diameter were prepared using the leftover melt from the first measurement. These ingots were cut into disk-shaped specimens 3 to 8 mm in height and cleaned with a 5%NaOH aqueous solution. The specimen was put on an insulating brick and re-melted using an infrared heater. Then, a chromel-alumel thermocouple 0.1 mm in diameter was inserted into the melt, and the melt temperature was controlled by the infrared heater. At 973 K, two chill plates placed at both sides were moved quickly toward the center to cool the melt. Spacer plates 2, 4 and 6 mm thick were used to maintain the minimum distance between the two chill plates. The chill plates were made of JIS-S50C steel or insulating brick. In these conditions, cooling curves with solidification times from 1 to 150 s were recorded at a sampling interval of 1 or 10 ms.

In the second measurement, the temperature distributions in the 6 mm thick specimens were also determined using three thermocouples, as shown in

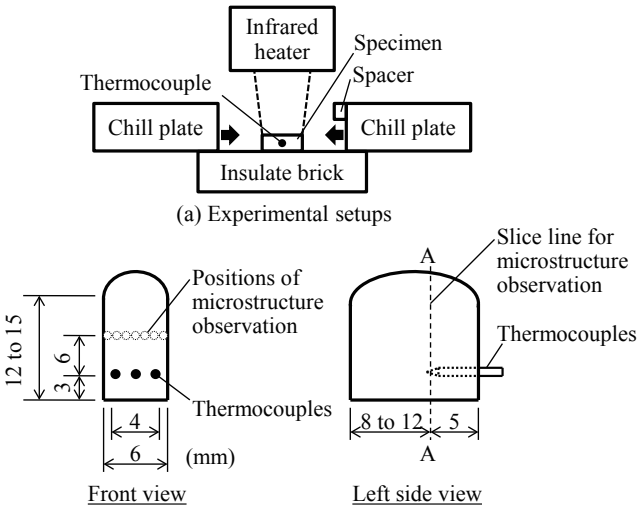

(b) Shape of the 6 mm thick specimen and the positions of temperature measurement and microstructure observation for measuring solid fraction.

Fig. 1 Drawings of the second cooling curve measurement.

Fig. 1(b). Some of the specimens were rapidly cooled by water before the completion of the solidification and cut at the A-A cross section shown in Fig. 1(b). Then, the microstructures were observed in the horizontal direction, and the solid fraction of each view was determined by image analysis to obtain the solid fraction distribution.

2. 2 Determination of Solidification Rate

The melt temperature T [K] as a function of time t [s] was obtained from the cooling curves as shown in **Fig. 2**. Their time differentials dT/dt [K·s^{-1}] were also plotted in the same figure. In many cooling curves, the recalescence phenomena (i.e., the increase in the melt temperature at the early stage of solidification) were found. The starting time of the eutectic solidification

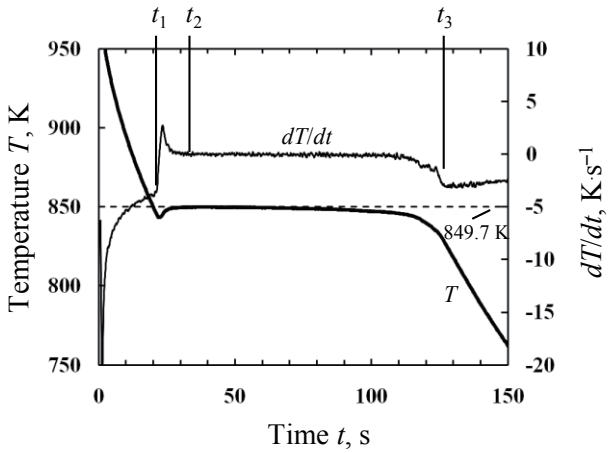

(a) Cooled by insulate brick plates

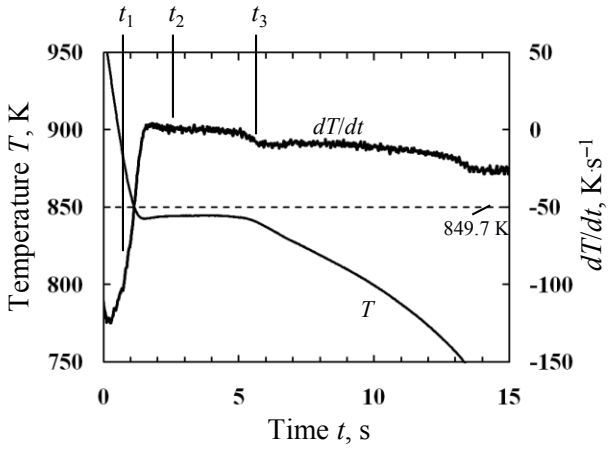

(b) Cooled by S50C steel plates

Fig. 2 Cooling curves of 6 mm thick specimens obtained by the second measurement.

t_1 is defined as the onset of the dT/dt curve found at the point just before recalescence. After this increase, the melt temperature shows the highest temperature of eutectic solidification T_{peak}, and $dT/dt = 0$ at this point. The time at which T_{peak} is reached is defined as t_2. The end time of the eutectic solidification can be defined by the time when dT/dt reaches the minimum value because this point is coincident with the final release of the latent heat. From these definitions, the solidification time t_f [s] is given by Eq. (1).

$$t_f = t_3 - t_1 \tag{1}$$

Note that when the chill plates were made of S50C steel, there were two minimum points of dT/dt (i.e., when the local solidification completed and when the melt entirely solidified because of the large temperature gradient in the specimen). In this case, the former is the time t_3.

Since the solid fraction F_s increases from 0 to 1 at the solidification time t_f, the average solidification rate $(dF_s/dt)_{ave}$ [s^{-1}] is given by the inverse of t_f.

$$\left(\frac{dF_s}{dt}\right)_{ave} = (1-0)/t_f = t_f^{-1} \tag{2}$$

On the other hand, the undercooling during eutectic solidification ΔT [K] is the temperature difference between the equilibrium temperature T_{eq} [K] and the melt temperature T [K].

$$\Delta T = T_{eq} - T \tag{3}$$

The equilibrium temperature T_{eq} was determined thermodynamically by the Thermo-Calc software[12] using Scheil's model.[13] **Figure 3** shows the relationship between T_{eq} and the solid fraction F_s of the Al-Si binary eutectic alloy and the Al-Si alloy whose composition is listed in Table 1. Although T_{eq} for the Al-Si binary eutectic alloy is constant at 850.1 K, T_{eq} for the commercial grade Al-Si alloy decreases from 849.7 to 845 K with an increase in the solid fraction because it contains a small amount of iron and other impurities. However, this decrease in T_{eq} is so small that T_{eq} is assumed to be constant at 849.7 K when $0 \leqq F_s \leqq 0.5$. Noting that the highest eutectic temperature T_{peak} usually appears at the early stage of eutectic solidification, the undercooling during eutectic solidification ΔT [K] can be described as follows:

$$\Delta T = 849.7 - T_{peak}. \quad (4)$$

A set of data for the average solidification rate and the undercooling was determined from the measured cooling curves for solidification times ranging from 1 to 1000 s by Eqs. (2) and (4). Then, the least squares method was applied to obtain an empirical function of the solidification rate dF_s / dt as follows:

$$\frac{dF_s}{dt} = f(\Delta T). \quad (5)$$

It must be noted that the solidification rate calculated by Eq. (5) indicates the maximum value for a given undercooling value because this undercooling is the minimum value determined at $t = t_2$. At the early and late stages of solidification, however, the solid-liquid boundary areas are much smaller than those of the middle stage due to the limitation of nucleation or the decrease in the left melt.[14] Thus, the solidification rate at these stages must be smaller than the values calculated by Eq. (5). In order to consider the decrease in the solidification rate, Eq. (5) is modified as follows:

$$\frac{dF_s}{dt} = f(\Delta T) \times N, \quad (6)$$

where N is a solidification rate parameter that satisfies $0 < N \leqq 1$ and is defined as a function of F_s. Here, $N = 1$ indicates the highest solidification rate, and $0 < N < 1$ gives the solidification rates at the early and late stages of solidification.

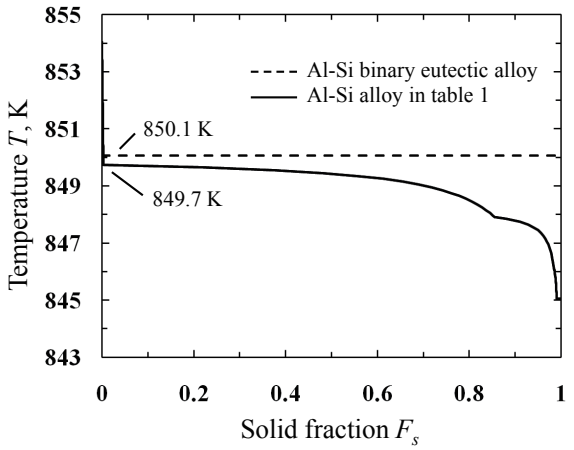

Fig. 3 Solid fraction-temperature relationships of the Al-Si binary eutectic alloy and the Al-Si alloy in Table 1 calculated with the Scheil module of the Thermo-Calc software.

It is important to note that an appropriate N value cannot be determined experimentally or theoretically by itself. Therefore, the N value was determined by comparing the solidification analysis results with the experimental results. In the next section, the calculation scheme and the way to determine the N value are described.

2. 3 Solidification Analysis

2. 3. 1 Calculation Scheme

The equation of heat conduction is given by

$$\int_V \rho c \frac{\partial T}{\partial t} dV = -\int_S q_n dS, \quad (7)$$

where q_n is the heat flux, ρ is the density, c is the specific heat, V is the control volume, and S is the control surface area. Equation (7) was explicitly solved by the finite volume method[15] to calculate the heat conduction without considering solidification or melting. In the cases of complete liquid or solid states, the temperature T^{n+1} at time step n+1 can be calculated from the known temperature T^n at time step n. In the case of a solid-liquid coexisting state, T^{n+1} is substituted by a temporal temperature T^* ignoring the release or absorption of latent heat. Solidification or melting was considered by the conventional temperature recovery method[16] and the modified temperature recovery method. Since the conventional temperature recovery method is an equilibrium model, the increment of the solid fraction ΔF_s for a time step is given by the slope of the T-F_s curve plotted in Fig. 3,

$$\Delta F_s = (T^n - T^*) \Big/ \left(\frac{L}{c} - \frac{dT}{dF_s} \right), \quad (8)$$

where L is the latent heat [J/kg], and dT /dF_s is the slope of the T-F_s curve. In the modified temperature recovery method, the undercooling ΔT of each control volume was calculated by Eq. (9).

$$\Delta T = T_{eq} - T^* \quad (9)$$

Then, ΔF_s is given by Eq. (10) using the solidification rate given by Eq. (6).

$$\Delta F_s = \frac{dF_s}{dt} \times \Delta t \quad (10)$$

Obviously, the modified temperature recovery

method is a non-equilibrium model that considers the undercooling and the solidification rate. In both the equilibrium and the non-equilibrium models, the temperature recovery due to the solidification or the melting at a particular time step is given by $(L/c)\,\Delta F_s$. Thus, T^{n+1} is written as shown in Eq. (11).

$$T^{n+1} = T^{*} + \frac{L}{c}\Delta F_s \tag{11}$$

2. 3. 2 Calculation Condition

Two-dimensional solidification analysis was conducted on the second cooling curve measurements in which a 6 mm thick specimen was cooled by chill plates made of S50C steel or insulating bricks. **Fig. 4** shows the computational domains and the boundary conditions. A rectangular coordinate system with square meshes was used for all calculations. The mesh sizes were changed from 0.3 to 0.5 mm in the case of an insulating brick and from 0.2 to 0.3 mm in the S50C steel case in order to evaluate the mesh size effect. The relationship of T-F_s for the commercial grade Al-Si eutectic alloy shown in Fig. 3 was used to calculate T_{eq}. The other material properties are listed in **Table 2**, and the initial temperatures of each domain are listed in **Table 3**.

As mentioned above, the N value in Eq. (6) for the non-equilibrium model must be determined by comparing the experimental and numerically calculated results. The boundary conditions should also be found in the same way. Therefore, some preliminary calculations concerning the solidification time were carried out to fix the heat transfer coefficients h_A and h_B, where an insulating condition at the other boundaries and a constant condition of $N = 1$ were assumed. The fixed h_A and h_B were listed in **Table 4**. Next, three levels of N in **Table 5** were set, and the appropriate values were determined from the comparison of the temperature and the solid fraction distributions. Finally, validation of this calculation was confirmed by comparing (1) the time-dependent temperature

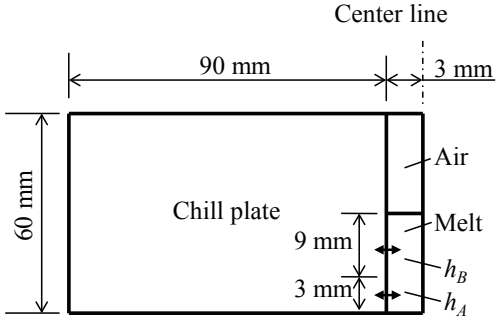

Fig. 4 Computational domains of the numerical simulations.

Table 2 Material properties used in the numerical simulations.

	Al-Si alloy in table 1	Insulate brick	S50C	Unit
Thermal conductivity	70	0.75	53.5	W/(m·K)
Density	2562	1800	7830	kg/m^3
Specific heat	1202	180	460.5	J/(kg·K)
Latent heat	505400			J/kg

Table 3 Initial temperatures used in the numerical simulations (K).

	Insulate brick	S50C
Melt	977.5	974.6
Chill plates	303	323

Table 4 Time-dependent heat transfer coefficients (Wm^{-2}K^{-1}).

Insulate brick			S50C		
Time (s)	h_A	h_B	Time (s)	h_A	h_B
0	500	125	0	4500	1400
21.8	400	333	1.5	3500	1000
			2.0	3000	800
			3.0	2400	700
			4.0	2000	600
			5.0	1800	600
			6.0	1600	600

Table 5 Parameter N considering the limited nucleation and growth.

	N			
	Fixed	Small	Middle	Large
$0 \le F_s < 0.0001$	1.0	0.00001	0.0001	0.01
$0.0001 \le F_s < 0.05$		0.1		
$0.05 \le F_s < 0.6$		1.0		
$0.6 \le F_s < 0.9$		0.8		
$0.9 \le F_s \le 1$		0.1		

distribution, (2) the solid fraction distribution, and (3) the influence of different solidification times.

3. Results

3. 1 Undercooling and Solidification Rate of Eutectic Solidification

From the first and second cooling measurements, it was found that the commercial grade Al-Si eutectic alloy solidified with the recalescence phenomena when the solidification time t_f was over 1.2 s. Therefore, the maximum eutectic solidification temperature T_{peak} can be determined in the same t_f range. As shown in **Fig. 5**, T_{peak} decreased as t_f became shorter when $t_f < 100$ s but was almost the same as the equilibrium temperature of 849.7 K.

Figure 6 shows the relationship between the average solidification rate $(dF_s/dt)_{ave}$ and the undercooling ΔT. It is clear that $(dF_s/dt)_{ave}$ increases as ΔT becomes larger. When $(dF_s/dt)_{ave} > 0.01$, the empirical function in Eq. (12) is obtained.

$$\frac{dF_s}{dt} = f(\Delta T) = 0.012\exp(0.58\Delta T) \qquad (12)$$

Substituting Eq. (12) for $f(\Delta T)$ in Eq. (6), the solidification rate can be calculated in the non-equilibrium model.

3. 2 Solidification Analysis with Regard to Temperature Distribution

Figure 7 shows the measured and calculated cooling curves for the 6 mm thick specimen cooled by S50C steel chill plates. The undercooling during the eutectic solidification was about 5 K. The non-equilibrium model can calculate this undercooling, while the eutectic solidification temperature is the same as the equilibrium temperature in the result of the equilibrium model. It is impossible to calculate the recalescence phenomena when $N = 1$. In contrast, the recalescence became larger with a decrease in N. In this case, the cooling curve calculated with a middle level of N is in accordance with the measured curve.

Figure 8 shows the temperature distribution of the same specimen calculated by the non-equilibrium model at the middle level of N with different mesh sizes. The solidification time near the chill plate is about 2 s and is much shorter than that of the center due to the large temperature gradient. There is a small influence of the mesh size on the calculation results, and the calculated undercooling at both of the two positions shows good agreement with the measured ones.

Figure 9 shows the measured and calculated cooling curves for the 6 mm thick specimen cooled by the insulating brick chill plates. Under this condition, the temperature difference in the specimen is about 0.3 K, and this is so small that only the temperature at the center of the specimen is shown in this figure. Although the undercooling at T_{peak} was small (about 0.1 K), about 6 K of undercooling was found at the

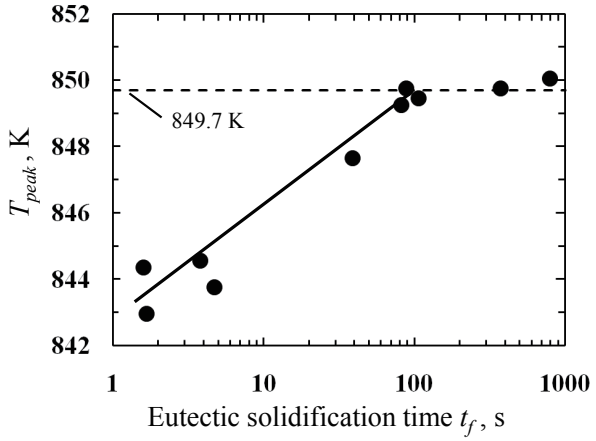

Fig. 5 Relationship between the eutectic solidification time t_f and the peak of the eutectic solidification temperature T_{peak} for the Al-Si alloy in Table 1.

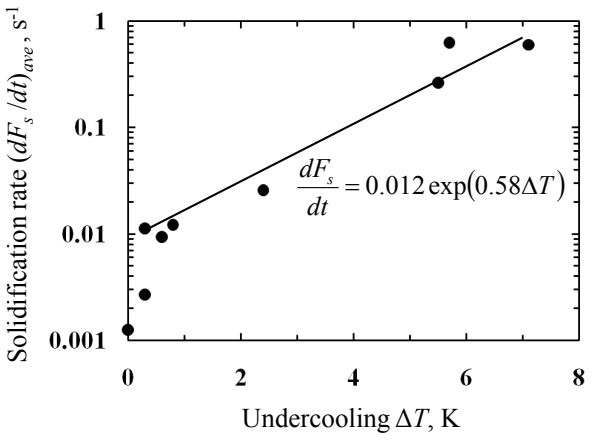

Fig. 6 Relationship between the undercooling DT at $t = t_2$ and the average solidification rate $(dF_s/dt)_{ave}$.

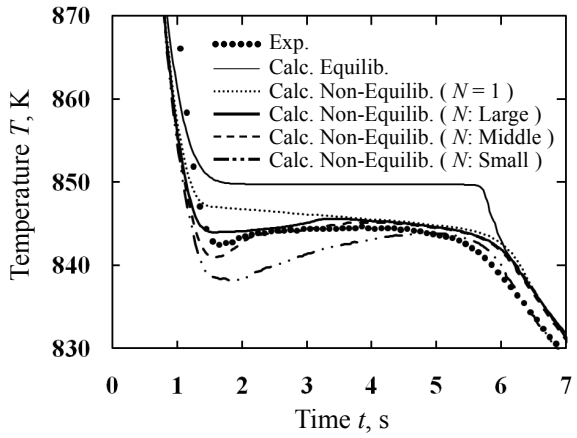

Fig. 7 Experimental and calculated cooling curves of a 6 mm thick specimen cooled by S50C plates.

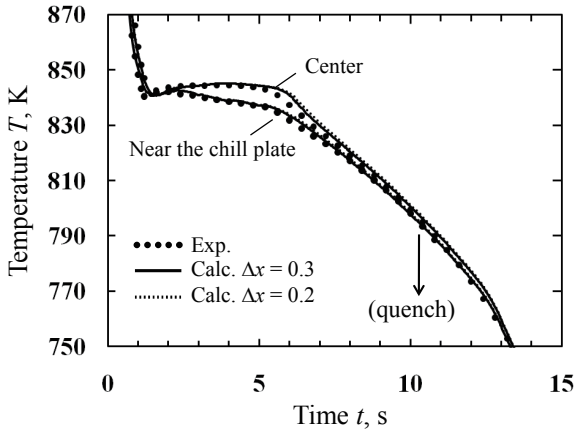

Fig. 8 Temperature distribution of a 6 mm thick specimen cooled by S50C plates and the influence of the mesh sizes calculated by the middle *N* level.

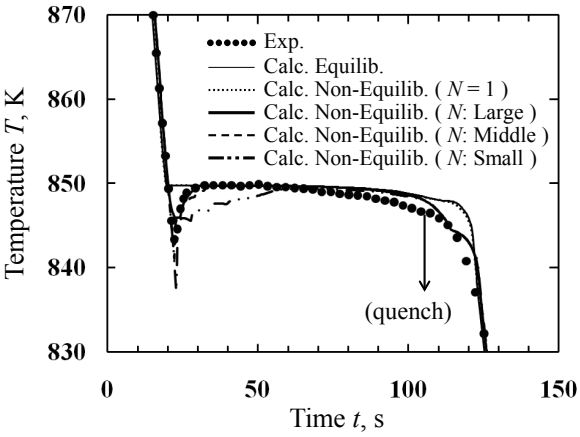

Fig. 9 Experimental and calculated cooling curves of a 6 mm thick specimen cooled by insulating brick plates.

early stage of the solidification. This recalescence phenomenon can be calculated by the non-equilibrium model at the middle level of *N*.

3. 3 Solidification Analysis with Regard to Distribution of Solid Fraction

Figure 10 shows the solidification structures at 9 mm from the bottom of the 6 mm thick specimens. These specimens were quenched at t = 105 s for the case of insulating brick chill plates and t = 10 s for the case of S50C steel chill plates, as shown in Fig. 9. It is obvious that the fine structures were liquid phase before quenching. Therefore, the area fraction of the fine structure was defined as the liquid fraction F_L, and thus the solid fraction $F_s = 1 - F_L$. In the case of insulating brick chill plates, F_s = 0.83 at the surface, and F_s = 0.53 at the center, which is a small difference due to a small temperature difference in the specimen. In the case of S50C steel chill plates, there is a larger solid fraction difference (i.e., F_s = 1.0 at the surface, and F_s = 0.36 at the center) because the temperature difference was large, as shown in Fig. 8.

The solid fraction distribution of these specimens was plotted in **Fig. 11**. The gradient of the solid fraction taken from the specimen cooled by insulating brick chill plates was smaller than that of the specimen cooled by S50C steel chill plates. Similar to this experimental result, the calculated solid fraction

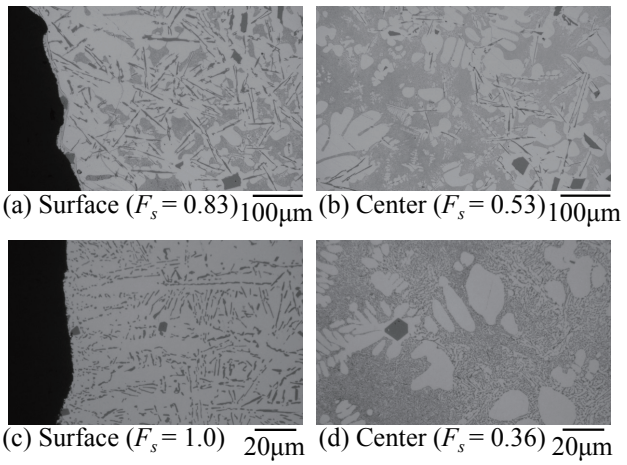

Fig. 10 Solidification structures of 6 mm thick specimens 9 mm from the bottom: (a) and (b) cooled by insulating brick plates and quenched at 105 s (see Fig. 9); (c) and (d) cooled by S50C plates and quenched at 10 s (see Fig. 8).

gradient became larger when the chill plate material was changed from the insulating brick to S50C steel. However, the calculation results clearly depend on the calculation models.

In the case of the insulating brick chill plates shown in Fig. 11(a), the gradient of the solid fraction calculated by the equilibrium model and the non-equilibrium model with $N = 1$ was smaller than the experimental result because these models overestimated the solidification from the melt at the center due to ignoring the limitation of nucleation. In contrast, the calculation result of the non-equilibrium model with the middle level of N agreed with the experimental results.

When S50C steel was used for the chill plates, a high cooling rate resulted from the high undercooling. However, since the undercooling is not taken into account in the equilibrium model, the calculated solid fraction distribution exhibited a skin formation type behavior and disagreed with the experimental result. Oppositely, the calculation result from the non-equilibrium model with $N = 1$ shows a smaller gradient of solid fraction, although the undercooling is considered in this model. One major cause is the overestimation of the solidification from the undercooled melt due to neglecting the limitation of nucleation. It seems that this problem can be avoided by changing the value of N. In this case, the gradient of the solid fraction calculated by the non-equilibrium model with the middle level of N agreed with the experimental results.

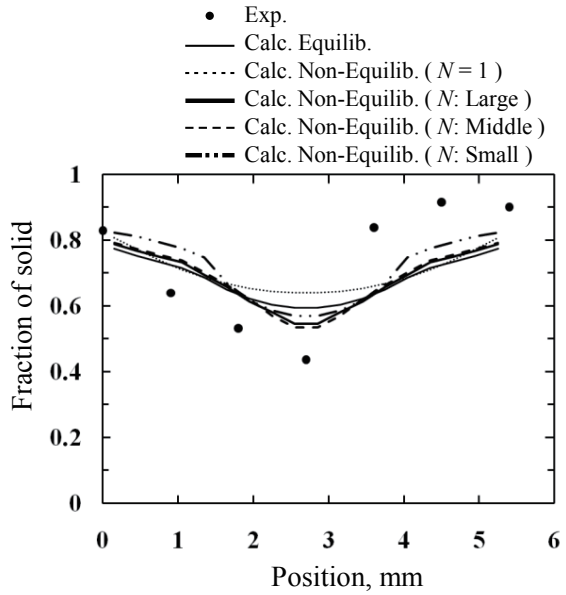

(a) Cooled by insulate brick plates

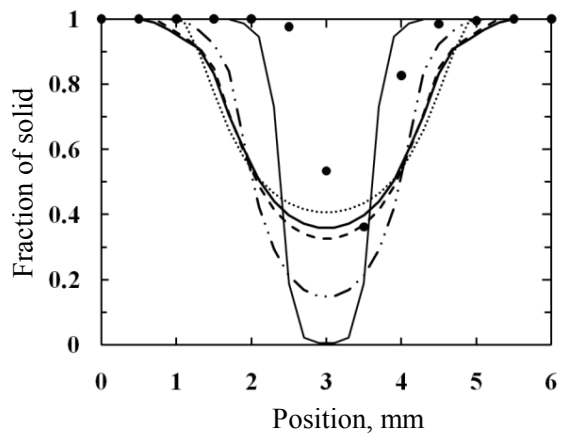

(b) Cooled by S50C plates

Fig. 11 Experimental and calculated solid fraction distributions of 6 mm thick specimens 9 mm from the bottom.

4. Discussion

4. 1 Validation of the Calculation Model

In the solidification analysis, there are three state values that express the thermal quantities of the solid-liquid coexisting condition: the temperature T, the enthalpy H, and the solid fraction F_s. The relationship between these state values is a material property and is described as follows:

$$H = cT + (1 - F_s)L\,, \tag{13}$$

where c is the specific heat, and L is the latent heat. Therefore, to determine the thermal state of an undercooled melt or solid-liquid coexisting state, it is necessary to fix at least two of the state values. In other words, validation of the calculation model can be confirmed by comparing two state values. In the previous section, good agreement of the time-dependent temperature distribution and the solid fraction distribution between the experiments and the non-equilibrium model with the middle level of N was obtained. Therefore, it can be said that the middle level of N is the most appropriate value, and the non-equilibrium model is suitable to calculate undercooled solidification.

4. 2 Solidification Modes of Al-Si Eutectic Alloy

It is known that Al-Si eutectic type alloys whose silicon content is near the eutectic composition solidify in the skin formation mode because their solidification range is so small that the solidified layer easily forms at their surfaces in normal casting conditions. However, the experimental results in Figs. 10 and 11 clearly showed that the solid fraction increased at both the surface and the center of the specimens. It has been reported that if melt undercooling and an effective nucleation site exist, eutectic cell formation mode solidification occurs when the temperature gradient is small.[1,7,8] There are some similarities in this solidification mode change and the columnar-to-equiaxed transition in the solidification of hypo-eutectic Al-Si alloys caused by constitutional undercooling and homo- or heterogeneous nucleation.[7,20] In this work, the undercooling was about 0.3 K for the specimen cooled by the insulating brick chill plates. According to TEM observations,[17,18] SEM observations,[8] and EDS mappings,[19] an AlP particle is the most likely nucleation site of eutectic silicon. Since commercial grade aluminum alloys usually contain phosphorous, there would be a lot of nucleation sites of eutectic silicon in the melt. Therefore, it is acceptable that the solid fraction increased at both the surface and the center of the specimens.

4. 3 Influence of Segregation on Distribution of Solid Fraction

Pure aluminum and Al-Si binary eutectic alloy that has no solidification range should solidify in the skin formation mode upon the assumption of equilibrium solidification. This solidification behavior is demonstrated by the Stephan problem, which is a theoretical analysis for the phase transformation of pure substances.[21] In practice, however, the existence of undercooling during solidification satisfies the requirements for the nucleation and growth of eutectic cells or equiaxed grains as mentioned above. In addition, the commercial grade Al-Si eutectic alloy used in this investigation contains some amount of impurities such as iron, which makes about a 5 K solidification range due to the micro-segregation, as shown in Fig. 3. When the temperature difference in the melt becomes smaller than this solidification range, the eutectic cells or equiaxed grains can nucleate and grow from the melt. The solidification of the 6 mm thick specimen cooled by insulating brick chill plates is the case in which the temperature difference along the horizontal direction is about 0.3 K. This means that not only the undercooling and the solidification rate but also the solidification range must be considered for solidification analysis in the non-equilibrium model.

5. Conclusion

This investigation was carried out for the development of a solidification analysis technique for Al-Si eutectic alloys that can consider undercooling and the solidification rate without an increase in calculation time. For this purpose, the solidification behavior of a commercial grade Al-Si binary eutectic alloy was first investigated. The temperature distribution, the solid fraction distribution, and the undercooling during the eutectic solidification of the alloy were determined by measuring the cooling curves and observing the solidification structures at various cooling rates. From these data, the solidification rate of the alloy was successfully derived. Secondly, a new calculation technique based on the modified temperature recovery method was proposed to consider the nucleation and growth from the undercooled melt. It was validated by comparing the temperature distribution and the solid fraction distribution between the experimental and calculated results.

(1) An empirical relationship between the solidification rate and undercooling was obtained as described by Eq. (12) for a commercial grade Al-Si binary eutectic alloy.

(2) A new calculation technique based on the modified temperature recovery method was proposed. This technique uses the solidification rate in Eq. (12) combined with the solidification rate parameter N, which makes it possible to consider the nucleation and growth from the undercooled melt.

(3) The validation of the proposed calculation technique was confirmed by comparing the experimental and calculated results of the time-dependent temperature distribution and the solid fraction distribution.

(4) The N of a middle level was the most appropriate value for the commercial grade Al-Si eutectic alloy used in this study.

References

(1) Nogita, K. and Dahle, A. K., *J. Jpn. Inst. Light Metals* (in Japanese), Vol. 54 (2004), pp. 440-446.
(2) Awano, Y., *J. Jpn. Inst. Light Metals* (in Japanese), Vol. 56 (2006), pp. 335-342.
(3) "Report of Dendrite Arm Spacing in Diecastings", (in Japanese) (1990), p. 123, Japan Foundry Society, Inc.
(4) Kato, E. et al., *J. Jpn. Inst. Light Metals* (in Japanese), Vol. 46 (1996), pp. 377-382.
(5) Morinaka, M., *J. Jpn. Foundry Eng. Soc*. (in Japanese), Vol. 75 (2003), pp. 325-330.
(6) Adachi, M., *J. Jpn. Inst. Light Metals* (in Japanese), Vol. 34 (1984), pp. 361-373.
(7) Dahle, A. K. et al., *Metall. Mater. Trans*. A, Vol. 32 (2001), pp. 949-960.
(8) Kadoi, K. et al., *J. Jpn. Foundry Eng. Soc*. (in Japanese), Vol. 82 (2010), pp. 203-211.
(9) Gandin, Ch.-A. and Rappaz, M., *Acta Metall. Mater*., Vol. 42 (1994), pp. 2233-2246.
(10) Cho, S. H. et al., *Sci. Technol. Adv. Mater*., Vol. 2 (2001), p. 241-245.
(11) Koroyasu, S. and Matsuda, M., *J. Jpn. Foundry Eng. Soc.* (in Japanese), Vol. 78 (2006), pp. 3-8.
(12) Sundman, B. et al., *CALPHAD*, Vol. 9 (1985), pp. 153-190.
(13) Scheil E., *Z. Metallk*., Vol. 34 (1942), pp.70-72
(14) Nakae, H., *Gyouko Kougaku* (in Japanese) (1987), p. 85, AGNE Gijutsu Center Inc.
(15) Hasuno, A. et al., *Trans. JSME B* (in Japanese), Vol. 61 (1995), pp. 1470-1476.
(16) Ohnaka, I., *Computer Dennetsu - Gyoko Kaiseki Nyumon* (in Japanese) (1985), p. 193, Maruzen.
(17) Dahle, A. K. et al., *Mater. Sci. Eng. A*, Vol. 413-414, (2005), pp. 243-248.
(18) Nogita, K. et al., *J. Electron. Microsc*., Vol. 53 (2004), pp. 361-369.
(19) Cho, Y. H. et al., *Metall. Mater. Trans*. A, Vol. 39 (2008), pp. 2435-2448.
(20) Heiberg, G. et al., *Acta Mater*., Vol. 50 (2002), pp. 2537-2546.
(21) Shouji, M., *Dennetsu Kougaku* (in Japanese) (1995), p. 77, University of Tokyo Press.

Figs. 1-11 and Tables 1-5
Reprinted from J. Jpn. Foundry Eng. Soc., Vol. 84, No. 4 (2012), pp. 185-192, Yaokawa, J., Iwata, Y., Amano, N. and Nakamichi, T., Undrecooled Solidification Analysis of Al-Si Eutectic Alloy with Consideration of Solidification Rate, © 2012 Japan Foundry Engineering Society.

Jun Yaokawa
Research Fields:
- Metal Casting
- Computer Aided Engineering

Academic Degree: Dr.Eng.
Academic Societies:
- Japan Foundry Engineering Society
- The Japan Institute of Metals and Materials

Award:
- The Best Paper Award of Japan Foundry Engineering Society, 2013

Yasushi Iwata
Research Fields:
- Metal Casting
- Computer Aided Engineering

Academic Degree: Dr.Eng.
Academic Society:
- Japan Foundry Engineering Society

Awards:
- Kobayashi Award of Japanese Foundry Society, 1989
- Onoda Award of Japan Die Casting Association, 1989
- The Best Paper Award of Japan Foundry Engineering Society, 2001, 2010 and 2013

Norihiro Amano*
Research Fields:
- Metal Casting
- Computer Aided Engineering

Academic Society:
- Japan Foundry Engineering Society

Award:
- The Best Paper Award of Japan Foundry Engineering Society, 2013

Takashi Nakamichi*
Research Fields:
- Metal Casting
- Computer Aided Engineering

Academic Societies:
- Japan Foundry Engineering Society

Awards:
- The Technology Prize of Japan Foundry Engineering Society, 2007
- The Best Paper Award of Japan Foundry Engineering Society, 2013

*Toyota Motor Corporation

